CONCRETE SLABS REINFORCED WITH FRP GRIDS. II: PUNCHING RESISTANCE

By Stijn Matthys[1] and Luc Taerwe[2]

ABSTRACT: The use of fiber-reinforced polymer (FRP) grid reinforcement for concrete slabs has been investigated, considering the behavior of the slabs in one-way bending and under concentrated loading. The behavior under the latter loading type will be considered in this second part of a two-part paper. From the performed punching tests and the analysis, a fairly strong interaction between shear and flexural effects was noted for most of the tested slabs. For the FRP-reinforced slabs with an increased reinforcement ratio or an increased slab depth (needed to fulfill the serviceability criteria in bending), the punching strength was similar to or higher than the tested steel-reinforced reference slabs. For most slabs, slip of the bars occurred resulting in higher deflections at failure. The calculation of the punching failure load according to empirical-based models (from different codes), a modified mechanical model, and an analytical model is evaluated.

INTRODUCTION

In recent years, there has been increasing interest in fiber-reinforced polymer (FRP) materials as nonmetallic reinforcement for concrete structures. However, due to the relatively low modulus of elasticity and the brittleness of FRP materials, its use for reinforced concrete members is less attractive than for prestressed members. In spite of these aspects, Matthys and Taerwe (2000) showed in part Part I of this two-part paper the feasibility of FRP grid reinforcement, if proper structural measures are considered, in terms of flexural behavior. For example, it was found that the design of the slabs is mainly determined by serviceability criteria. As a further investigation it is also of interest to study the problem of punching shear in connection with flat-slab floor systems and certain bridge deck configurations. In this sequel, experimental and analytical work will be presented. Punching shear of concrete slabs reinforced or externally strengthened with FRP also is addressed by Ahmed et al. (1994), Bank and Xi (1995), Banthia et al. (1995), Erki and Heffernan (1995), and Matthys and Taerwe (1996).

EXPERIMENTAL PROGRAM

A total of 17 punching tests have been performed on square slabs with a side length of 1,000 mm and a total slab depth of 120 or 150 mm. These slabs, except for two additionally cast reference slabs (R2 and R3), were obtained from remaining specimens (width of 1,000 mm, total depth of 120 or 150 mm, and total length of 4,500 mm) tested in four-point bending. After the bending tests, saw-cuts were made at a distance of 1 m from each slab end. Due to the previous bending test, the specimens show three to five preexisting cracks. The mean crack width $w_{m,ini}$ of these cracks is given in Table 1. The test specimens are subdivided in three series: the first series with steel-reinforced reference slabs (series R); the second series with different types of carbon FRP (CFRP) grids (series C/CS); and the third series with a hybrid type of FRP comprising both glass and carbon fibers (series H). Different diameters for the loading area also were used. An overview of the characteristics of the different test specimens is given in Table 1.

The following types of reinforcement were used: steel mesh reinforcement (S500, ribbed bars), a CFRP mesh (CFRP Carbon-Stress with a diameter of 5 mm and a sanded surface), and NEFMAC grids of type C (carbon fibers) and type H (mixture of glass and carbon fibers). These latter grids are characterized by a fairly smooth surface of the bars (negligible bond along the bars), so that mechanical anchorage of the bars is assured by the transverse bars. The characteristics of the reinforcement are given in Table 2. More details on the FRP reinforcement (including stress-strain curves) can be found in Part I. For the slabs, a normal-strength concrete (mean compressive cylinder strength $f_{cm} \approx 30$ MPa at 28 days) was used, except for slab H1, which was cast with high-strength concrete (HSC) ($f_{cm} \approx 95$ MPa). The concrete strengths also are given in Table 1.

The square concrete slabs were tested in a vertical position according to the test setup depicted in Fig. 1. They were supported by eight supports located along a circle with a diameter of 0.9 m (Fig. 1). The load was applied at the center on a circular load patch with a diameter as indicated in Table 1. The slabs were positioned in such a way that initial cracks were located at the tension side. During the tests, the applied load, central deflection, radial strains, circumferential strains, crack development, and crack widths were measured. After testing, the slabs were sawn in two orthogonal directions, parallel to the directions of the reinforcement, to study the failure mode and to verify the location of the load patch relative to the location of the grid (Fig. 2).

TEST RESULTS

Ultimate Load

The results of the tests are given in Table 3, in terms of failure load Q_u and corresponding nominal shear stress

$$\tau_{n,\eta d} = \frac{Q_u}{u_{\eta d} d} \tag{1}$$

where $u_{\eta d}$ = control perimeter at a distance ηd from the edge of load patch (in Europe η is often taken as 1.5 or 2 and in North-America as 0.5). Furthermore, the following general characteristics also are given or repeated in Table 3: the mean initial crack width $w_{m,ini}$, the equivalent reinforcement ratio $\rho E_r/E_s$, and the flexural stiffness in the fully cracked state (proportional to $E_r A_r d^2$).

From the observed failure loads the following is noted:

- For equal load patch diameters, increasing failure loads are found with increasing flexural stiffness.

[1]Ir., Res. Asst. IWT, Magnel Lab. for Concrete Res., Dept. of Struct. Engrg., Ghent Univ., Technologiepark-Zwijnaarde 9, B-9052 Gent, Belgium. E-mail: StijnMatthys@rug.ac.be

[2]Prof. Dr. Ir., Magnel Lab. for Concrete Res., Dept. of Struct. Engrg., Ghent Univ., Technologiepark-Zwijnaarde 9, B-9052 Gent, Belgium.

Note. Discussion open until January 1, 2001. Separate discussions should be submitted for the individual papers in this symposium. To extend the closing date one month, a written request must be filed with the ASCE Manager of Journals. The manuscript for this paper was submitted for review and possible publication on January 21, 1999. This paper is part of the ***Journal of Composites for Construction***, Vol. 4, No. 3, August, 2000. ©ASCE, ISSN 1090-0268/00/0003-0154–0161/$8.00 + $.50 per page. Paper No. 20102.

TABLE 1. Characteristics of Test Specimens

Slab (1)	$w_{m,ini}$ (mm) (2)	f_{cm}[a] (MPa) (3)	Age at test (days) (4)	Diameter load patch (mm) (5)	Slab depth (mm) (6)	Mean effective depth d (mm) (7)	Reinforcement type (8)	Bar spacing (mm) (9)	Reinforcement ratio ρ (%) (10)
R1/R1′	0.02/0.06	33.5	466/835	150/230	120	90	ϕ10 mm S500	150	0.58
R2[b]	0[b]	35.1	237	150	120	88	ϕ12 mm S500	100	1.29
R3[b]	0[b]	35.1	363	150	120	86	ϕ14 mm S500	100	1.79
C1/C1′	0.15/0.21	30.4	470/817	150/230	120	96	Grid type C10	150	0.27
C2/C2′	0.07/0.05[c]	29.6	444/805	150/230	120	95	Grid type C16	100	1.05
C3/C3′	0.07/0.07[c]	28.0	442/799	150/230	150	126	Grid type C13	100	0.52
CS/CS′	0.07/0.09	27.2	376/722	150/230	120	95	ϕ5 mm CFRP S	110	0.19
H1	0.30	96.7	678	150	120	95	Grid type H10	150	0.62
H2/H2′	0.05/0.08	29.3	685/757	150/80	120	89	Grid type H19	100	3.76
H3/H3′	0.10/0.10	26.3	651/723	150/80	150	122	Grid type H16	150	1.22

[a]Mean compressive cylinder strength of concrete at 28 days.
[b]New-cast slabs (no initial flexural cracks).
[c]For slabs C2′ and C3′, respectively, one and three of the initial cracks extent over total depth.

TABLE 2. Characteristics of Reinforcement

	According to Manufacturer			Obtained from Tensile Tests		
Reinforcement (1)	Sectional area (mm^2) (2)	Tensile strength (MPa) (3)	Modulus of elasticity (MPa) (4)	Tensile strength (MPa) (5)	Modulus of elasticity[a] (MPa) (6)	Ultimate strain (mm/m) (7)
S500						
ϕ10 mm	78.5	500[b]	200,000	620[b]	200,000	82.5
ϕ12 mm	113.1	500[b]	200,000	619[b]	200,000	—[d]
ϕ14 mm	153.9	500[b]	200,000	589[b]	200,000	—[d]
Grid type						
C10	39.2	1,180	98,100	1,690	91,800	17.6
C13	65.0	1,180	98,100	1,350	92,000	12.8
C16	100.0	1,180	98,100	1,340	95,000	13.6
H10	88.8	520	36,300	665	37,300	16.1
H16	223.0	520	36,300	640	44,800	12.9
H19	335.0	520	36,300	(555)[c]	40,700	(13.8)[c]
CFRP, ϕ5 mm	19.6	2,400	160,000	2,300	147,600	14.1

[a]Tangent modulus (determined between strain points 1 and 3 mm/m).
[b]Yield stress.
[c]Anchorage failure (pull out).
[d]Not available.

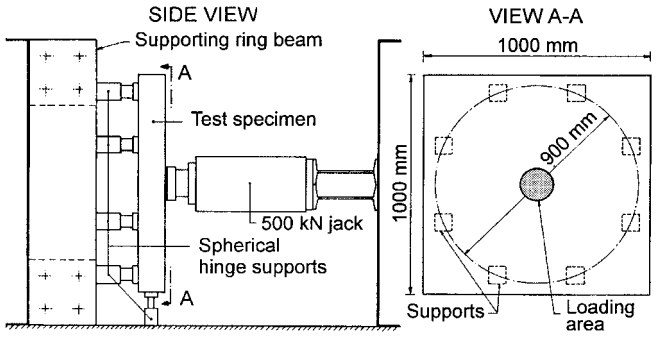

FIG. 1. Test Setup

- Comparing slabs with similar flexural stiffness, the effect of an increased slab depth on the punching resistance seems to be more pronounced than the effect of an increased reinforcement ratio (e.g., comparing slabs C1/C2 and C1/C3, whereas slabs C2 and C3 have similar flexural stiffness but different depths and reinforcing ratios).
- FRP-reinforced concrete slabs designed with a similar flexural strength as reference slab R1 and hence a lower flexural stiffness (see Part I) have significantly lower punching strengths (slabs R1, C1, and CS). Slabs designed with a similar flexural stiffness as slab R1 have similar or higher punching strengths for series C (slabs R1, C2, and C3) and slightly lower punching strengths for series H (slabs R1, H2, and H3). Hence, to obtain similar punching resistance as steel-reinforced slabs, the FRP-reinforced slabs should have a flexural stiffness that is sufficiently high.
- Comparing the failure loads of slabs with similar effective depths and different types of flexural reinforcement, the obtained failure loads are roughly similar for equal equivalent reinforcement ratios $\rho E_r/E_s$ (comparing slabs R1/C2/H2 or C1/CS). A similar comparison between slabs C3 and H3 (same total depth) indicates a significant lower failure load for slab H3. However, for this slab the effective depth also is lower (Table 1).
- Higher failure loads are found with increasing load patch diameter (except for slab C3′, due to its higher initial damage level. However, this effect is less pronounced than the influence of the reinforcement ratio and the slab depth.
- Slab H1 with HSC failed in bending and has a higher punching resistance than slabs C1 and CS (with similar equivalent reinforcement ratio and flexural stiffness).

Failure Mode

Fig. 3 shows the cracking pattern at failure of slabs C1 and CS. Herein, the dashed lines indicate the initial cracks (see the section Experimental Program). As the slabs were loaded, a

J. Compos. Constr., 2000, 4(3): 154-161

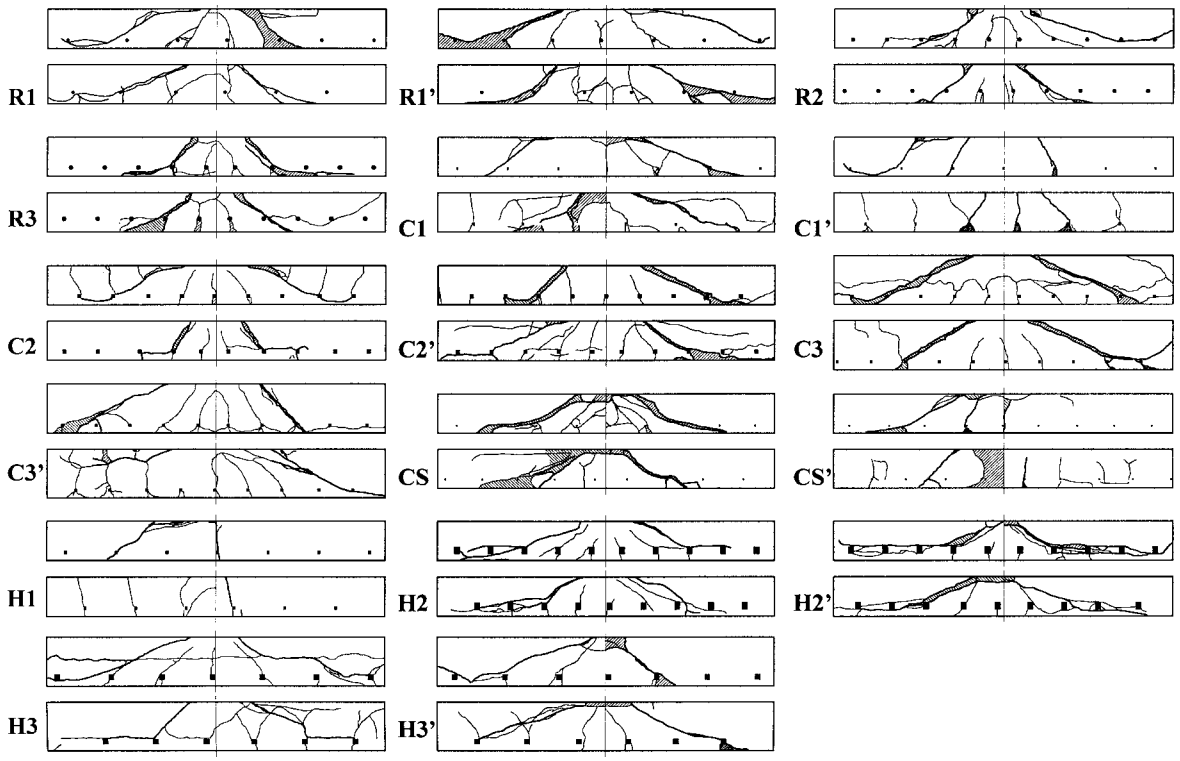

FIG. 2. Cross Section and Crack Pattern of Slabs

TABLE 3. Test Results

Slab (1)	$w_{m,ini}$ (mm) (2)	$\rho E_r/E_s$ (%) (3)	$E_r A_r d^2$ (10^{12} N·mm^2) (4)	Q_u (kN) (5)	$\tau_{n,0.5d}$ (MPa) (6)	$\tau_{n,1.5d}$ (MPa) (7)	Failure mode (8)	Q_u/Q_f (9)	Q_u/Q_p (10)	r_{cone} (mm) (11)	α_{cone} (degrees) (12)
R1	0.02	0.58	0.85	240	3.54	2.02	P	1.05	0.47	239 ± 56	29
R1′	0.06	0.58	0.85	265	2.93	1.87	P	1.04	0.51	347 ± 63	21
R2	0[a]	1.29	1.75	294	4.47	2.57	P	0.66	0.57	223 ± 91	31
R3	0[a]	1.79	2.28	313	4.91	2.84	P	0.58	0.61	166 ± 16	42
C1	0.15	0.12	0.24	181	2.44	1.37	P	1.01	0.35	281 ± 57	25
C1′	0.21	0.12	0.24	189	1.92	1.21	F/P	0.90	0.37	—	—
C2	0.07	0.50	0.89	255	3.49	1.96	P	0.69	0.49	224 ± 90	32
C2′	0.05[b]	0.50	0.89	273	2.81	1.78	P	0.62	0.53	279 ± 59	30
C3	0.07	0.24	1.01	347	3.18	1.66	P	0.78	0.50	327 ± 33	27
C3′	0.07[b]	0.24	1.01	343	2.43	1.43	P	0.65	0.49	340 ± 101	29
CS	0.07	0.14	0.26	142	1.94	1.09	P	0.87	0.28	251 ± 49	28
CS′	0.09	0.14	0.26	150	1.55	0.98	P/F	0.78	0.29	256 ± 50	34
H1	0.30	0.12	0.19	207	2.83	1.59	F/P	1.26	0.25	—	—
H2	0.05	0.77	0.96	231	3.46	1.98	P	0.63	0.45	273 ± 39	24
H2′	0.08	0.77	0.96	171	3.62	1.76	P	0.57	0.33	202 ± 54	29
H3	0.10	0.27	0.80	237	2.27	1.20	P	0.52	0.34	292 ± 91	29
H3′	0.10	0.27	0.80	217	2.80	1.27	P	0.58	0.31	301 ± 98	25

Note: P = punching cone failure; F/P = mixed failure, mainly flexural; P/F = mixed failure, mainly punching.
[a]New-cast slabs (no initial flexural cracks).
[b]For slabs C2′ and C3′, respectively, one and three of the initial cracks extent over total depth.

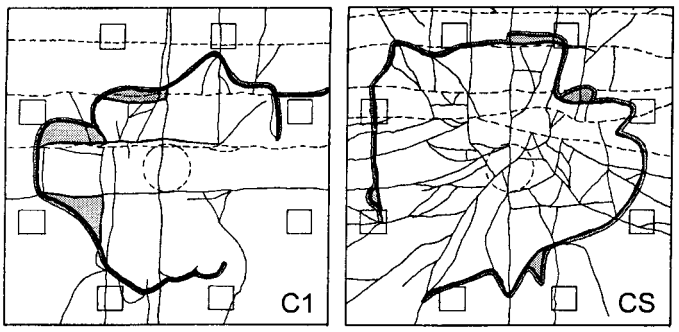

FIG. 3. Crack Patterns at Ultimate of Slabs C1 and CS (Tension Side)

series of cracks developed from the center of the slabs and extended toward the edges. Although originally following the direction of the reinforcement, at higher load levels these radial cracks, for the slabs with good bond characteristics along the bars (slabs R and CS), radiated in all directions. At the same time some circumferential cracks, connecting the radial cracks, were formed (Fig. 3). For the other slabs (negligible bond along the bars, the transverse bars ensure a mechanical anchorage of the longitudinal bars and vice versa), the crack extensions basically followed the direction of the reinforcement, appearing rather suddenly over the total width of the slab and with large initial crack widths due to fairly extensive slipping of the bars, which could be observed at the edge coinciding with the saw-cut. For these slabs, mostly no circum-

J. Compos. Constr., 2000, 4(3): 154-161

ferential cracking occurred (Fig. 3). Prior to failure, damage for all the slabs was dominated by two (or three) wide cracks running parallel to the directions of the grid reinforcement and extending over the total slab width. This indicates a flexural behavior. However, at the ultimate load, a punching cone developed for nearly all the slabs (Fig. 2). This failure cone extends from the edge of the load patch to the tensile side of the slab where it appears as a circumferential crack. For slabs C1′, CS′, and H1 a mixed failure occurred (Fig. 2 and Table 3).

For all slabs, slip of the flexural reinforcement was noticed. Depending on the bond behavior (respectively good or negligible bond along the bars), slip occurred near failure or shortly after cracking. In the latter case, for grids with large bar spacing, slip resulted in a sudden crack appearance with high initial crack widths. In general, slip of the bars resulted in less brittle punching failures.

From the above observations, it follows that a strong interaction occurred for the tested slabs between flexural and shear effects. This aspect was verified analytically, by calculating the flexural capacity Q_f and the pure punching shear capacity Q_p of the slabs. Herein, Q_f is calculated based on a yield line analysis for the slabs with steel reinforcement and an elastic analysis (Bareš 1979) for the slabs with FRP reinforcement. The flexural moment capacity per unit width of the slabs was calculated as described in Part I (with $\varepsilon_{cu} \leq 5.5$ mm/m). The pure punching shear capacity Q_p (when flexural effects are neglected) is calculated by means of an upper-bound plastic analysis (Nielsen 1984). Table 3 gives the obtained ratios Q_u/Q_f and Q_u/Q_p. These clearly show that the obtained punching cone failures are close to flexural failures, especially for the slabs with low reinforcement ratios.

Punching Cone Shape

Fig. 2 shows the cross sections of the slabs in two orthogonal directions (parallel with the flexural reinforcement) and the measured crack pattern. Typically, the slabs failing with a punching cone were not damaged at the compression side, except for the load patch indention. Furthermore, it is noticed (Fig. 2) that the punching cone shear crack often follows the flexural reinforcement layer for some distance before reaching the concrete surface at the tension side as a circumferential crack. This aspect may be attributed to slip of the flexural reinforcement and spalling of the concrete cover.

Based on the measured shear cracks (Fig. 2), the mean distance r_{cone}, from the center to the intersection of the shear crack and the flexural reinforcement, has been determined. This cone radius and its standard deviation (based on four measurements) are given in Table 3, as well as the corresponding cone angle α_{cone} (assuming a perfect cone extending from the load patch and with radius r_{cone} at the reinforcement level). Although subject to considerable variation, the observed angles agree with values reported for other test programs (''Punching'' 1985). The mean angle for slabs R, C/CS, and H equals 30.7°, 29.2°, and 26.8°, respectively. The latter value may indicate that a lower modulus of elasticity of the flexural reinforcement slightly decreases the cone angle.

Deflections

The load-deflection behavior of the slabs is shown in Figs. 4–6. For the slabs with low FRP reinforcement ratios (similar flexural strength as the steel-reinforced reference slab R1), the punching failure load is considerably less than the reference slab R, except for slab H1 with HSC. At the same time these slabs show low stiffness in the cracked state resulting in deflections that are twice as large as those of the other slabs. By increasing the FRP reinforcement ratio and/or the slab depth

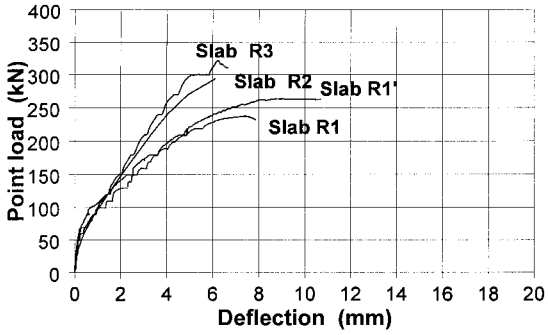

FIG. 4. Load Deflection Behavior of Slabs R

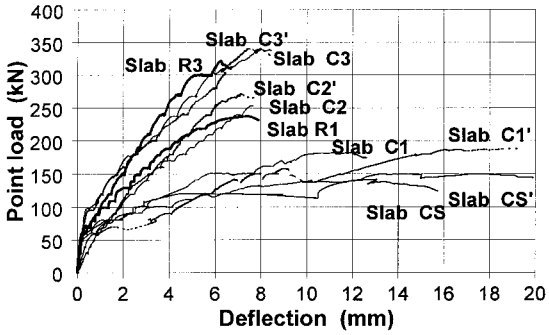

FIG. 5. Load Deflection Behavior of Slabs R1, R3, and C/CS

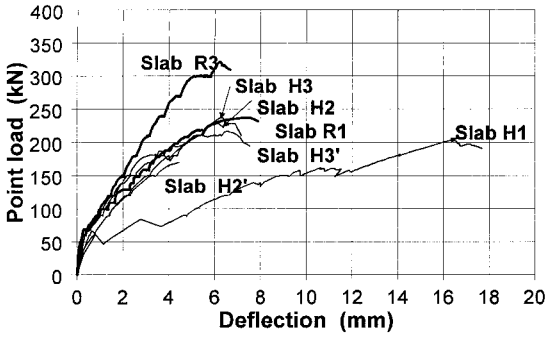

FIG. 6. Load Deflection Behavior of Slabs R1, R3, and H

[needed to match the serviceability criteria in flexural bending (see Part I)], a similar behavior is obtained between the different series.

THEORETICAL VERIFICATION

Code Equations (Empirical-Based Models)

The ultimate loads obtained for all the slabs were verified by calculation of the punching capacity according to CEB-FIP Model Code 1990 (MC90) [Comité Euro-International du Béton (CEB) 1993], Eurocode 2 (EC2) [Comité Européen de Normalisation (CEN) 1991], the Japanese Society of Civil Engineers (JSCE) (*Recommendation* 1997), and ACI 318-95 [American Concrete Institute (ACI) 1995], which are basically empirical-based formulas. The design value of the punching resistance, according to these codes, is defined as follows:

$$Q_{d,\text{MC90}} = 0.12\xi \sqrt[3]{100\rho f_{ck}}\, u_{2d} d \leq 0.3 \left(1 - \frac{f_{ck}}{250}\right) f_{cd} u_0 d \quad (2)$$

where

$$\xi = 1 + \sqrt{\frac{200}{d}} \ (d \text{ in mm})$$

J. Compos. Constr., 2000, 4(3): 154-161

$$Q_{d,\mathrm{EC2}} = 0.025\,\frac{f_{ctk}}{\gamma_c}\,k(1.2 + 40\rho)u_{1.5d}d \tag{3}$$

where

$$k = (1.6 - d) \geq 1 \ (d \text{ in meter}); \quad \rho \leq 0.015$$

$$Q_{d,\mathrm{JSCE}} = \beta_d\beta_p\beta_r\,\frac{f_{pcd}}{\gamma_b}\,u_{0.5d}d \tag{4}$$

where

$f_{pcd} = 0.2\sqrt{f_{cd}} \leq 1.2$ MPa; $\beta_d = \sqrt[4]{1/d} \leq 1.5$ (d in meter);

$\beta_p = \sqrt[3]{100\rho} \leq 1.5$; $\beta_r = 1 + 1/(1 + 0.25u_0/d)$

$$Q_{d,\mathrm{ACI}} \leq \varphi(1 + 2/\beta_c)(\sqrt{f'_c}/6)u_{0.5d}d$$

$$\leq \varphi\left(\frac{\alpha_s d}{2u_{0.5d}} + 1\right)(\sqrt{f'_c}/6)u_{0.5d}d$$

$$\leq 2\varphi(\sqrt{f'_c}/6)u_{0.5d}d \tag{5}$$

where

$$f'_c \leq 35 \text{ MPa}$$

In (2)–(5), ρ and d = mean reinforcement ratio and effective depth, respectively; f_{cm}, f_{ck}, f_{cd}, and f'_c = mean, characteristic, design, and specified compressive strengths of the concrete, respectively; f_{ctk} = characteristic tensile strength of the concrete; $u_{\eta d}$ = control perimeter at a distance ηd from the load patch; u_0 = perimeter of the load patch; γ_c = partial safety factor for the concrete strength equal to 1.5; γ_b = member factor equal to 1.3 or 1.5, respectively, for concrete strengths below and above 50 MPa; β_c = ratio of long side to short side of the concentrated load (1 if circular shaped); α_s = constant equal to 40 for interior columns (or concentrated loads); and φ = strength reduction factor equal to 0.85.

In addition, the empirical expression [(6)] has been included in the verification. This expression corresponds to a comprehensive analysis of several codes and test programs as presented in CEB Bulletin 168 (''Punching'' 1985). A similar approach by Gardner (1990) resulted in basically the same formula

$$Q_{emp} = 1.36\,\frac{(100\rho f_{cm})^{1/3}}{d^{1/4}}\,u_{1.5d}d \tag{6}$$

where $u_{1.5d}$ = rectangular or square control perimeter at a distance $1.5d$ from the load patch (regardless of whether the load area is rectangular or circular in section).

In the first instance, the mean punching capacity was calculated as follows. In (2)–(5), mean values of the concrete strength were considered and partial safety factors (γ_c, γ_b, and ϕ) were set equal to 1. For (2), a safety factor γ_c incorporated in the constant 0.12 was assumed. Hence, this constant was multiplied with $\gamma_c = 1.5$ to obtain the mean punching capacity. The results are given in Table 4 (under the heading ''M'') and Fig. 7. Although subject to considerable scatter, per reinforcement type (series R, C/CS, and H, respectively), all models predict the punching capacity in a consistent way, whereas the mean ratio of the ultimate load to the predicted load Q_u/Q_{pred} differs for the three series. For series R (steel reinforcement) this ratio is about 1.2–1.9, indicating some additional safety by the models, although mean values of the concrete strength and safety factors equal to 1 were used in the calculation. Lower values for the mean ratio Q_u/Q_{pred} are found for series C/CS and H, about 0.9–1.3 and about 0.7–1.5, respectively. Especially for series H, with a very low modulus of elasticity of the grid reinforcement, the punching strength is overestimated (except for the ACI equation). In general, a similar trend is noticed for all models when comparing the mean ratio Q_u/Q_{pred} for the different series, except for the ACI equation, which neglects the influence of the flexural reinforcement.

In view of the low ratios Q_u/Q_{pred} obtained for FRP reinforcement, a second calculation of the mean punching capacity was performed taking into account the axial rigidity of the reinforcement by substituting the reinforcement ratio ρ by the equivalent ratio $\rho E_r/E_s$, as also specified by JSCE (*Recommendation* 1997). By doing so (Table 4 under the heading ''Mm'' and Fig. 7), safer predictions and less scatter are obtained. Also, per model, the mean ratio Q_u/Q_{pred} for the different series is roughly similar now.

TABLE 4. Theoretical Verification (Empirical-Based Models)

Slab (1)	Q_u (kN) (2)	Failure mode (3)	Q_u/Q_{MC90}			Q_u/Q_{EC}			Q_u/Q_{JSCE}			Q_u/Q_{ACI}		Q_u/Q_{emp}	
			M (4)	Mm (5)	Dm (6)	M (7)	Mm (8)	Dm (9)	M (10)	Mm (11)	Dm (12)	M (13)	D (14)	M (15)	Mm (16)
R1	240	P	1.30	1.30	2.09	1.32	1.32	2.83	1.55	1.55	2.56	1.67	2.20	1.26	1.26
R1′	265	P	1.23	1.23	1.98	1.21	1.21	2.59	1.37	1.37	2.26	1.37	1.80	1.16	1.16
R2	294	P	1.25	1.25	2.01	1.12	1.12	2.40	1.49	1.49	2.46	2.08	2.74	1.21	1.21
R3	313	P	1.22	1.22	1.97	1.17	1.17	2.50	1.46	1.46	2.41	2.27	2.98	1.19	1.19
Mean			1.25	1.25	2.01	1.20	1.20	2.58	1.47	1.47	2.42	1.85	2.43	1.20	1.20
C1	181	P	1.19	1.54	2.50	0.80	0.84	1.79	1.43	1.85	3.10	1.21	1.61	1.15	1.49
C1′	189	F/P	1.07	1.39	2.26	0.70	0.73	1.57	1.20	1.56	2.61	0.94	1.26	1.01	1.31
C2	255	P	1.09	1.40	2.28	0.98	1.13	2.43	1.32	1.69	2.85	1.75	2.35	1.06	1.36
C2′	273	P	1.01	1.29	2.11	0.88	1.01	2.17	1.14	1.46	2.45	1.40	1.88	0.95	1.22
C3	347	P	1.27	1.65	2.70	1.05	1.14	2.45	1.50	1.94	3.29	1.64	2.22	1.24	1.61
C3′	343	P	1.11	1.44	2.36	0.89	0.97	2.08	1.22	1.59	2.68	1.25	1.68	1.06	1.37
CS	142	P	1.11	1.23	2.02	0.87	0.88	1.90	1.37	1.51	2.57	1.02	1.39	1.08	1.19
CS′	150	P/F	1.01	1.12	1.85	0.77	0.78	1.67	1.16	1.29	2.19	0.80	1.09	0.96	1.06
Mean			1.11	1.38	2.26	0.87	0.94	2.01	1.29	1.61	2.72	1.25	1.69	1.06	1.33
H1	207	F/P	0.72	1.26	1.93	0.56	0.66	1.41	1.03	1.81	2.90	1.27	1.69	0.70	1.22
H2	231	P	0.71	1.20	1.97	0.97	1.16	2.48	0.90	1.47	2.48	1.73	2.33	0.69	1.17
H2′	171	P	0.83	1.03	1.69	0.86	1.03	2.20	0.85	1.39	2.33	1.81	2.43	0.61	1.04
H3	237	P	0.70	1.15	1.89	0.77	0.99	2.12	0.83	1.37	2.34	1.20	1.64	0.68	1.12
H3′	217	P	0.84	1.18	1.94	0.81	1.04	2.24	0.93	1.53	2.62	1.48	2.02	0.72	1.18
Mean			0.76	1.16	1.88	0.79	0.97	2.09	0.91	1.51	2.53	1.50	2.02	0.68	1.15

Note: P = punching cone failure; F/P = mixed failure, mainly flexural; P/F = mixed failure, mainly punching; M = based on mean values (no safety factors); D = based on design values (including safety factors); m = taking into account modification $\rho E_r/E_s$.

J. Compos. Constr., 2000, 4(3): 154-161

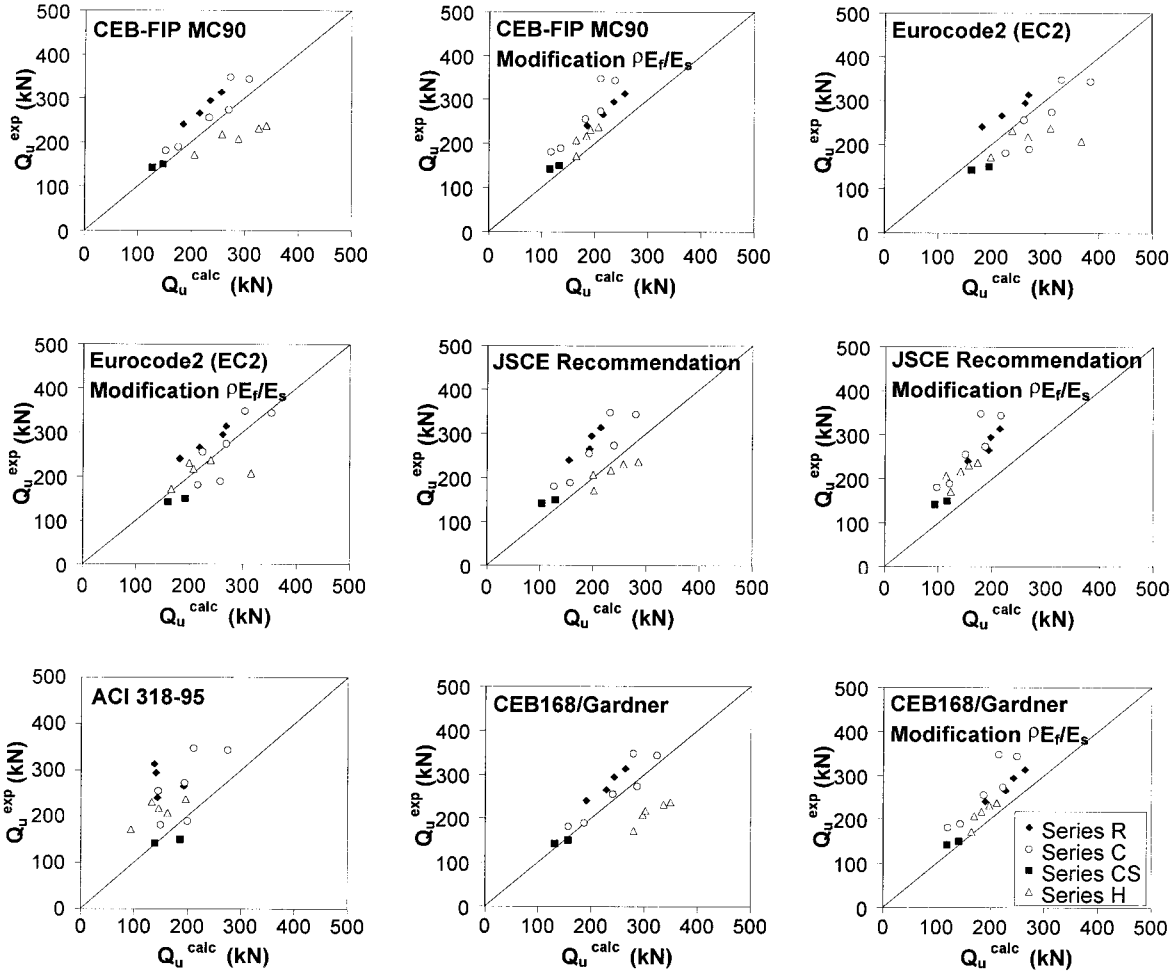

FIG. 7. Analytical Verification (Empirical-Based Models)

TABLE 5. Global Safety Factor

Slabs (1)	Mean Ratio $Q_u/Q_{m,d}$ and Standard Deviation			
	MC90 (2)	EC2 (3)	JSCE (4)	ACI 318 (5)
Series R	2.01 ± 0.06	2.58 ± 0.18	2.42 ± 0.13	2.43 ± 0.53
Series C/CS	2.26 ± 0.27	2.01 ± 0.33	2.72 ± 0.36	1.69 ± 0.45
Series H	1.88 ± 0.11	2.09 ± 0.40	2.53 ± 0.23	2.02 ± 0.36
All slabs	2.09 ± 0.26	2.17 ± 0.39	2.59 ± 0.30	1.96 ± 0.52

Finally, the global safety factor as provided by the code equations was determined by calculating the ratio of the failure load to the design capacity [as given in (2)–(5)] taking into account the axial rigidity of the reinforcement by the equivalent reinforcement ratio $\rho E_r/E_s$. Results for each slab are given in Table 4 (under the heading ''Dm''); mean values and standard deviations for the different series are given in Table 5. In general, all code equations are giving safe predictions, with a mean global safety factor of 2.0–2.6. Per code, the global safety factor is similar for the different types of reinforcement.

Modified Mechanical Model

A mechanical model for punching proposed by Hallgren (1996), based on the earlier model by Kinnunen and Nylander (1960) also was used to verify the test results. This model is based on the equilibrium of forces acting on a polar-symmetrical slab supported by a column. Herein, the slab portions that are outside the circumferential punching crack and formed by the radial crack are assumed to rotate as rigid bodies. Punching failure is obtained after reaching maximum principal confining stress of the multiaxial state of compressive stresses at the root of the punching cone. At that moment the cone shear crack runs through the compression zone. This failure criterion is modeled based on nonlinear fracture mechanics. Furthermore, the model considers dowel action of the flexural reinforcement. The model is not considering possible effects of slip of the flexural reinforcement.

For the analysis of the slabs reinforced with FRP grids, the model was modified to take the linear elastic behavior of the FRP reinforcement into account. Dowel action for the FRP reinforcement was considered to be negligible. Furthermore, the radius of the punching cone at the position of the flexural reinforcement r_{cone} was taken at a distance $1.8d$ of the load patch, as originally suggested by Kinnunen and Nylander (1960). This corresponds to an angle α_{cone} of 29°, which is close to the obtained experimental values (Table 3) [the modified formulation for r_{cone} by Hallgren (1996) was less accurate for both steel and FRP reinforcement and was not further adopted]. The model also was revealed to be rather insensitive to limited changes of α_{cone} (between 25° and 35°).

According to this modified mechanical model, fairly accurate predictions are obtained, as shown in Table 6 and Fig. 8. Furthermore, the scatter in the predictions is lower compared to most code equations.

Analytical Model Based on Numerical Simulations

Although good results are obtained with the modified mechanical model, the algorithm is an iterative process that involves a computer program. Therefore, a more simplified analytical model, proposed by Menétrey (1996) based on

J. Compos. Constr., 2000, 4(3): 154-161

TABLE 6. Theoretical Verification (Mechanical-Based Models)

Slab (1)	Q_u (kN) (2)	Failure mode (3)	Modified Mechanical Model (Hallgren 1996)		Analytical Model (Menétrey 1996)[a]			
			Q_u/Q_{mech} (4)	Reinforcement at ultimate (5)	$Q_u/Q_{34°}$ (6)	$Q_u/Q_{m,34°}$ (7)	$Q_u/Q_{29°}$ (8)	$Q_u/Q_{m,29°}$ (9)
R1	240	P	1.10	Yielding over total width[b]	2.65	2.65	2.08	2.08
R1′	265	P	1.08	Yielding over total width[b]	2.59	2.59	2.07	2.07
R2	294	P	1.03	Elastic state	2.16	2.16	1.69	1.69
R3	313	P	1.04	Elastic state	2.13	2.13	1.67	1.67
Mean			1.06		2.38	2.38	1.88	1.88
C1	181	P	1.34	No fracture (elastic state)	2.03	2.34	1.59	1.83
C1′	189	F/P	1.07	No fracture (elastic state)	1.89	2.18	1.51	1.74
C2	255	P	1.20	No fracture (elastic state)	1.94	2.53	1.52	1.98
C2′	273	P	0.95	No fracture (elastic state)	1.85	2.42	1.48	1.93
C3	347	P	1.25	No fracture (elastic state)	2.51	3.10	1.93	2.39
C3′	343	P	0.95	No fracture (elastic state)	2.23	2.75	1.75	2.16
CS	142	P	0.93	No fracture (elastic state)	2.11	2.21	1.65	1.73
CS′	150	P/F	0.74	No fracture (elastic state)	1.98	2.08	1.58	1.66
Mean			1.05		2.07	2.45	1.63	1.93
H1	207	F/P	0.95	No fracture (elastic state)	1.93	2.87	1.51	2.24
H2	231	P	0.97	No fracture (elastic state)	1.67	2.25	1.30	1.76
H2′	171	P	0.97	No fracture (elastic state)	1.44	1.95	1.10	1.48
H3	237	P	0.74	No fracture (elastic state)	1.49	2.42	1.15	1.87
H3′	217	P	0.87	No fracture (elastic state)	1.55	2.53	1.17	1.90
Mean			0.90		1.62	2.40	1.25	1.85

Note: P = punching cone failure; F/P = mixed failure, mainly flexural; P/F = mixed failure, mainly punching.
[a]For cone angles 34° and 29°, excluding or including modification $\rho E_r/E_s$.
[b]This indicates flexural failure instead of punching failure of slabs.

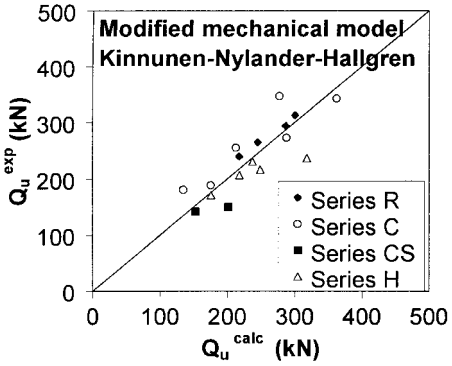

FIG. 8. Analytical Verification (Hallgren 1996)

findings of a finite-element analysis, also was used to verify the test results. This model defines the punching resistance of the concrete proportional to $f_{ctm}^{2/3}$, with f_{ctm} the concrete tensile strength. The real punching resistance is then obtained by multiplication factors to consider the size effects and the influence of the percentage of flexural reinforcement.

Results of the calculations according to this model are given in Table 6 and Fig. 9. The calculation is performed for two cone angles—34° [as suggested by Menétrey (1996) according to EC2 (CEN 1991)] and 29° [according to Kinnunen and Nylander (1960)]. Furthermore, the modified reinforcement ratio $\rho E_r/E_s$ was taken into account to model for the FRP reinforcement. From these calculations the following is noticed:

- Introduction of the modified reinforcement ratio $\rho E_r/E_s$, to model the use of FRP reinforcement, gives better predictions (similar ratios Q_u/Q_{pred} as for steel reinforcement) and less scatter.
- The model is largely dependent on the assumption of the cone angle.
- The model considerable underestimates the experimental results for the steel- and FRP-reinforced slabs [mean ratio $Q_u/Q_{m,29°}$ equals 1.9 (Table 6)].

CONCLUSIONS

The punching capacity of slabs reinforced in flexure with different types of FRP grid reinforcement was studied and compared to similar slabs with steel reinforcement. From the experimental and theoretical investigations the following conclusions can be drawn:

- For the tested specimens, a fairly strong interaction between shear and flexural effects has been found. However, most slabs showed a punching cone failure.
- The bond behavior of the grids was of considerable influence on the crack development and brittleness of the punching failure.

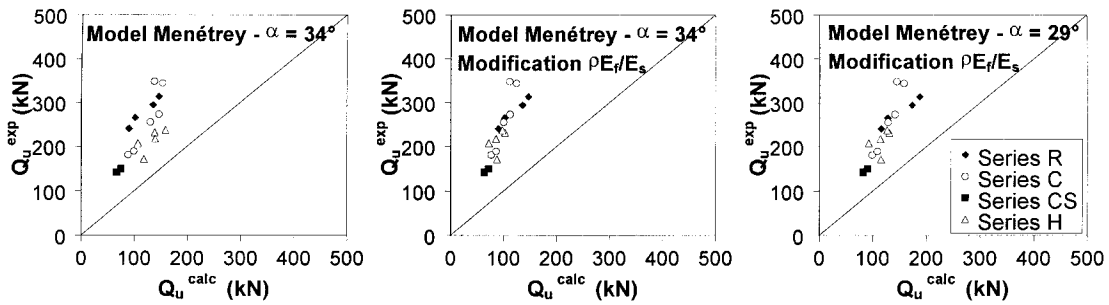

FIG. 9. Analytical Verification (Menétrey 1996)

J. Compos. Constr., 2000, 4(3): 154-161

- For the FRP-reinforced slabs with a similar flexural strength as the steel-reinforced reference slabs, the obtained punching load and stiffness in the cracked state were considerably less. However, for the FRP-reinforced slabs with an increased reinforcement ratio or an increased slab depth (flexural stiffness in the fully cracked state comparable to the reference slabs, needed to fulfill the serviceability criteria in bending), the behavior of the slabs was comparable to steel-reinforced reference slabs.
- The calculation of the mean punching failure load according to empirical-based expressions (such as most code equations) gives fairly good predictions, but with an underestimation for slabs with FRP reinforcement with low modulus of elasticity. The latter aspect was solved by introducing the equivalent reinforcement ratio $\rho E_r/E_s$.
- Evaluation of the design punching capacity according to the code equations, taking into account the modification $\rho E_r/E_s$, showed sufficient safety (mean global safety factor of about 1.9–2.6) for all investigated codes. Prediction according to MC90 gives a mean global safety factor of 2.1 and the least scatter.
- A modified mechanical model by Hallgren (1996) gives good results in predicting the behavior of steel- and FRP-reinforced slabs. A more simplified model by Menétrey (1996) is largely dependent on the assumption of the core angle and underestimates the punching capacity considerably.

APPENDIX I. REFERENCES

Ahmed, S. H., Zia, P., Yu, T. J., and Xu, Y. (1994). ''Punching shear tests of slabs reinforced with 3-D carbon fibre fabric.'' *Concrete Int.*, 16(6), 36–41.

American Concrete Institute (ACI). (1995). ''Building code requirements for structural concrete'' and ''Commentary.'' *ACI 318M-95* and *ACI 318RM-95*, Farmington Hills, Mich.

Bank, L. C., and Xi, Z. (1995). ''Punching shear behaviour of pultruded FRP grating reinforced concrete slabs.'' *Proc., 2nd Int. Symp. on Non-Metallic (FRP) Reinforcement for Concrete Struct.*, L. Taerwe, ed., E & FN Spon, London, 360–367.

Banthia, N., Al-Asaly, M., and Ma, S. (1995). ''Behavior of concrete slabs reinforced with fiber-reinforced plastic grid.'' *J. Mat. in Civ. Engrg.*, ASCE, 7(4), 252–257.

Bareš, R. (1979). *Tables for the analysis of plates, slabs and diaphragms based on the elastic theory*, Bauverlag GmbH, Wiesbaden and Berlin, Germany.

Comité Européen de Normalisation (CEN). (1991). ''Design of concrete structures, part 1.1: General rules and rules for buildings.'' *Eurocode 2*, Brussels.

Comité Euro-International du Béton (CEB). (1993). *CEB-FIP model code 1990*, Lausanne, Switzerland.

Erki, M.-A., and Heffernan, P. J. (1995). ''Reinforced concrete slabs externally strengthened with fibre-reinforced plastic materials.'' *Proc., 2nd Int. Symp. on Non-Metallic (FRP) Reinforcement for Concrete Struct.*, L. Taerwe, ed., E & FN Spon, London, 509–516.

Gardner, N. J. (1990). ''Relationship of the punching shear capacity of reinforced concrete slabs with concrete strength.'' *ACI Struct. J.*, 87(1), 66–71.

Hallgren, M. (1996). ''Punching shear capacity of reinforced high strength concrete slabs.'' PhD thesis, *TRITA-BKN. Bull. 23*, Royal Institute of Technology, Stockholm.

Kinnunen, S., and Nylander, H. (1960). ''Punching of concrete slabs without shear reinforcement.'' *Trans., Royal Inst. of Technol.*, Stockholm, No. 158.

Nielsen, M. P. (1984). *Limit analysis and concrete plasticity*, Prentice-Hall, Englewood Cliffs, N.J., 364–377.

Matthys, S., and Taerwe, L. (1996). ''Punching shear behaviour of concrete slabs reinforced with FRP grids.'' *Proc., 2nd Int. Conf. on Advanced Compos. Mat. in Bridges and Struct.*, M. El-Badry, ed., Canadian Society of Civil Engineers, Montreal, 261–270.

Matthys, S., and Taerwe, L. (2000). ''Concrete slabs reinforced with FRP grids. I: One-way bending.'' *J. Compos. for Constr.*, ASCE, 4(3), 145–153.

Menétrey, Ph. (1996). ''Analytical computation of the punching strength of reinforced concrete.'' *ACI Struct. J.*, 93(5), 503–511.

''Punching shear in reinforced concrete.'' (1985). *CEB Bull. d'Information No. 168*, Comité Euro-International du Béton, Lausanne, Switzerland.

Recommendation for design and construction of concrete structures using continuous fibre reinforcing materials. (1997). *Concrete Engrg. Ser. 23*, Japan Society of Civil Engineering, Tokyo.

APPENDIX II. NOTATION

The following symbols are used in this paper:

A_r = cross section of reinforcement;
d = mean effective depth;
E_r, E_s = moduli of elasticity of reinforcement (FRP or steel) and steel, respectively;
f'_c = specified concrete compressive strength;
f_{cm}, f_{ck}, f_{cd} = mean, characteristic, and design concrete compressive cylinder strengths, respectively;
f_{ctm}, f_{ctk} = mean and characteristic concrete tensile strengths, respectively;
K = flexural stiffness of fully cracked section;
Q_d, $Q_{m,d}$ = design punching capacities according to specified code, excluding or including the modification $\rho E_r/E_s$, respectively;
Q_{emp}, Q_{mech} = ultimate loads according to empirical-based model (''Punching'' 1985; Gardner 1990) or mechanical-based model (Hallgren 1996), respectively;
Q_f, Q_p = flexural capacity and pure punching shear capacity, respectively;
Q_{MC90}, Q_{EC2}, Q_{JSCE}, Q_{ACI} = punching capacities according to MC90, EC2, JSCE, and ACI 318, respectively, based on mean (M) or design (D) values and, if specified, including (Mm, Dm) modification $\rho E_r/E_s$;
Q_{pred} = predicted ultimate load;
Q_u = ultimate load (experimentally obtained);
Q_α, $Q_{m,\alpha}$ = ultimate loads according to analytical model (Menétrey 1996), for a cone angle α, excluding and including modification $\rho E_r/E_s$, respectively;
r_{cone} = punching cone radius at level of flexural reinforcement;
$u_{\eta d}$ = control perimeter at distance ηd from load patch (or column);
u_0 = perimeter of load area;
$w_{m,ini}$ = mean initial crack width of predamaged slabs;
α_{cone} = punching cone angle;
α_s = constant equal to 40 for interior columns (or concentrated loads);
β_c = ratio of long side to short side of the concentrated load (1 if circular shaped);
γ_c, γ_b = partial safety factors on concrete strength and member factor, respectively;
ε_{cu} = ultimate concrete compressive strain;
η = multiplier (indicating distance ηd, in function of effective depth d);
ρ = reinforcement ratio (per unit slab width);
$\rho E_r/E_s$ = equivalent reinforcement ratio;
$\tau_{n,\eta d}$ = nominal shear stress at control perimeter $u_{\eta d}$; and
ϕ = strength reduction factor or diameter.